

BLACK HOLE – NEUTRON STAR MERGERS AS CENTRAL ENGINES OF GAMMA-RAY BURSTS

H.-THOMAS JANKA¹, THOMAS EBERL^{1,2}, MAXIMILIAN RUFFERT³, AND CHRIS L. FRYER⁴

Draft version May 19, 2019

ABSTRACT

Hydrodynamic simulations of the merging of stellar mass black hole – neutron star binaries (BH/NS) are compared with mergers of binary neutron stars (NS/NS). The simulations are Newtonian, but take into account the emission of gravitational waves and their backreaction on the hydrodynamics. The use of a physical nuclear equation of state allowed us to include the effects of neutrino emission by a neutrino trapping scheme. For low neutron star to black hole mass ratios the neutron star transfers mass to the black hole during a few cycles of orbital decay and subsequent widening before finally being disrupted, whereas for ratios near unity the neutron star is already destroyed during its first approach. A gas mass between $\sim 0.3 M_{\odot}$ and $\sim 0.7 M_{\odot}$ is left in an accretion torus around the black hole and radiates neutrinos at a luminosity of several 10^{53} erg/s. The emitted neutrinos and antineutrinos annihilate into e^{\pm} pairs with efficiencies of a few percent and rates of up to $\sim 2 \times 10^{52}$ erg/s, releasing an estimated energy of up to $\sim 10^{51}$ erg in a pair-plasma fireball, which could give rise to a gamma-ray burst.

Subject headings: binaries: close — black hole physics — gamma-rays: bursts — stars: neutron

1. INTRODUCTION

BH/NS mergers are estimated to occur with daily event rates of about 500 in the universe and could be 5 times more frequent than NS/NS mergers (for recent numbers, see Fryer, Woosley, & Hartmann 1999; Bethe & Brown 1998, 1999). They are strong sources of gravitational waves (GWs) to be measured with the upcoming large interferometers (LIGO, VIRGO, GEO600, TAMA) and are considered as promising candidates for the origin of gamma-ray bursts (GRBs) (e.g., Blinnikov et al. 1984; Eichler et al. 1989; Paczyński 1991; Narayan, Piran, & Shemi 1992; Mészáros 1999), at least for the subclass of less complex and less energetic short and hard bursts (Mao, Narayan, & Piran 1994) with durations of fractions of a second (Popham, Woosley, & Fryer 1999; Ruffert & Janka 1999). Optical counterparts and afterglows of these have not yet been observed.

Newtonian SPH simulations of BH/NS mergers in which the neutron star is described by a polytropic equation of state, $P = K\rho^{1+1/n}$, K and n being constants, indicate that the neutron star may slowly lose gas in mass transfer cycles during hundreds of orbits (Klužniak & Lee 1998; Lee & Klužniak 1998, 1999). The question whether dynamical instability sets in at a minimum separation (Rasio & Shapiro 1994; Lai, Rasio, & Shapiro 1994) or whether stable Roche lobe overflow takes place, however, can depend on the neutron star to black hole mass ratio and the properties of the nuclear equation of state, expressed by the adiabatic index n (Uryū & Eriguchi 1999). Due to possibly long accretion time scales and the fact that a region of very low baryon density may exist above the poles of the black hole, BH/NS mergers are considered as more favorable source of GRBs than NS/NS mergers (e.g., Portegies Zwart 1998; Brown et al. 1999).

In this *Letter* we report about the first Newtonian BH/NS merger simulations (Eberl 1998) which were done with a realistic nuclear equation of state (Lattimer & Swesty 1991) and

which therefore yield information about the thermodynamic evolution and the neutrino emission of the neutron star matter. The simulations allow one to compare the strength of the GW emission relative to NS/NS mergers and to investigate neutrino-antineutrino ($\nu\bar{\nu}$) annihilation as potential source of energy for GRBs.

2. NUMERICAL METHODS

The three-dimensional hydrodynamic simulations were performed with a Eulerian PPM code using four levels of nested cartesian grids which ensure a good resolution near the center of mass and a large computational volume simultaneously. Each grid had 64^3 zones, the size of the smallest zone was 0.64 or 0.78 km in case of NS/NS and 1.25 or 1.5 km for BH/NS mergers. The zone sizes of the next coarser grid levels were doubled to cover a volume of 328 or 400 km side length for NS/NS and 640 or 768 km for BH/NS simulations. GW emission and its backreaction on the hydrodynamics were taken into account by the method of Blanchet, Damour, & Schäfer (1990) (see also Ruffert, Janka, & Schäfer 1996). The neutrino emission and corresponding energy and lepton number changes of the matter were calculated with an elaborate neutrino leakage scheme (Ruffert, Janka, & Schäfer 1996), and $\nu\bar{\nu}$ annihilation around the merger was evaluated in a post-processing step (Ruffert et al. 1997).

3. SIMULATIONS

Table 1 gives a list of computed NS/NS and BH/NS merger models. Besides the baryonic mass of the neutron star and the mass of the black hole, the spins of the neutron stars were varied. “Solid” means synchronously rotating stars, “none” irrotational cases and “anti” counter-rotation, i.e., spin vectors opposite to the direction of the orbital angular momentum. The cool neutron stars have a radius of about 15 km (Ruffert, Janka, & Schäfer 1996) and the runs were started with a center-to-center distance of 42–46 km for NS/NS and with 47 km in case

¹Max-Planck-Institut für Astrophysik, Postfach 1523, D-85748 Garching, Germany; thj@mpa-garching.mpg.de

²Technische Universität München, Physik-Department E12, James-Franck-Strasse, D-85748 Garching, Germany; thomas.eberl@physik.tu-muenchen.de

³Department of Mathematics and Statistics, University of Edinburgh, Scotland, EH9 3JZ, U.K.; m.ruffert@ed.ac.uk

⁴UCO/Lick Observatory, University of California, Santa Cruz, CA 95064, U.S.A.; cfryer@ucolick.org

of BH/NS for $M_{\text{BH}} = 2.5 M_{\odot}$, 57 km for $M_{\text{BH}} = 5 M_{\odot}$ and 72 km for $M_{\text{BH}} = 10 M_{\odot}$. The simulations were stopped at a time t_{sim} between 10 ms and 20 ms. The black hole was treated as a point mass at the center of a sphere with radius $R_s = 2GM_{\text{BH}}/c^2$ which gas could enter unhindered. Its mass and momentum were updated along with the accretion of matter. Model TN10, which is added for comparison, is a continuation of the NS/NS merger model B64 where at time $t_{\text{sim}} = 10$ ms the formation of a black hole was assumed and the accretion was followed for another 5 ms until a steady state was reached (Ruffert & Janka 1999).

4. RESULTS

4.1. Evolution of BH/NS mergers

Due to the emission of GWs the orbital separation decreases. During its first approach, the neutron star transfers matter to the black hole at huge rates of several 100 up to $\sim 1000 M_{\odot}/\text{s}$. Within 2–3 ms it loses 50–75% of its initial mass. In case of the $2.5 M_{\odot}$ black hole the evolution is catastrophic and the neutron star is immediately disrupted. A mass of 0.2 – $0.3 M_{\odot}$ remains in a thick disk around the black hole (M_d in Table 2). In contrast, the orbital distance increases again for $M_{\text{BH}} = 5 M_{\odot}$ and $M_{\text{BH}} = 10 M_{\odot}$ and a significantly less massive neutron star begins a second approach. Again, the black hole swallows gas at rates of more than $100 M_{\odot}/\text{s}$. Even a third cycle is possible (Fig. 1). Finally, at a distance d_{ns} and time t_{ns} the neutron star with a mass of $M_{\text{ns}}^{\text{min}}$ is destroyed and most of its mass ends up in an accretion disk (Table 2). (In case of NS/NS mergers t_{ns} means the time when the two density maxima of the stars are a stellar radius, i.e., $d_{\text{ns}} = 15$ km, apart).

The increase of the orbital separation is connected with a strong rise of the specific (orbital) angular momentum of the gas (Fig. 1). Partly this is due to the fact that the black hole can capture gas with low specific angular momentum first, but mainly because only a fraction of the orbital angular momentum of the accreted gas is fed into spinning up the black hole. This fraction, which is lost for the orbital motion, is proportional to the quantity α in Fig. 2. Figure 2 is based on the parameterized analysis of non-conservative mass-transfer by Podsiadlowski, Joss, & Hsu (1992) (see also Fryer et al. 1999) assuming that mass ejection from the system is negligible. It shows that for small initial black hole mass the orbital separation can increase only after the neutron star has lost mass, while for larger initial M_{BH} and smaller α orbital widening is easier. The separation increases when $\alpha < (M_{\text{BH}} - M_{\text{NS}})/(M_{\text{BH}} + M_{\text{NS}})$, which is fulfilled right to the minima of the curves corresponding to a certain value of α , because the black hole (neutron star) mass has grown (decreased) enough. A comparison with the simulations, taking into account the angular momentum loss by GW emission, suggests that α is between 0.2 and 0.5.

During the merging a gas mass ΔM_{ej} of $\sim 10^{-4} M_{\odot}$ (in case of counter-rotation and $M_{\text{BH}} = 2.5 M_{\odot}$) to $\sim 0.1 M_{\odot}$ (corotation and $M_{\text{BH}} = 10 M_{\odot}$) is dynamically ejected (Table 2). In the latter case the associated angular momentum loss is about 7%, in all other cases it is less than 5% of the total initial angular momentum of the system. Another fraction of up to 24% of the initial angular momentum is carried away by GWs. In Table 2 the rotation parameter $a = Jc/(GM^2)$ is given for the initial state of the binary system (a_i) and at the end of the simulation (a_f) for the remnant of NS/NS mergers or for the black hole in BH/NS systems, respectively, provided the black hole did not have any initial spin. When the whole disk mass M_d has been swallowed by the Kerr black hole, a final value a_{BH}^{∞} (Table 2)

will be reached in case of the accretion of a corotating, thin disk with maximum radiation efficiency.

The phase of largest mass flow rate to the black hole (between 2 and 5 ms after the start of the simulations) is connected with a maximum of the GW luminosity L_{GW} which reaches up to 7×10^{55} erg/s (Table 1). The peak values of L_{GW} and the wave amplitude rh (for distance r from the source) increase with the black hole mass. The total energy E_{GW} radiated in GWs can be as much as $0.1 M_{\odot}c^2$ for $M_{\text{BH}} = 10 M_{\odot}$.

4.2. Neutrino Emission and GRBs

Compressional heating, shear due to numerical viscosity, and dissipation in shocks heat the gas during accretion to maximum temperatures kT^{max} of several 10 MeV. Average temperatures are between 5 and 20 MeV, the higher values for the less massive and more compact black holes. At these temperatures and at densities of 10^{10} – 10^{12} g/cm³ in the accretion flow, electrons are non-degenerate and positrons abundant. Electron neutrinos and antineutrinos are therefore copiously created via reactions $p + e^- \rightarrow n + \nu_e$ and $n + e^+ \rightarrow p + \bar{\nu}_e$ and dominate the neutrino energy loss from the accreted matter. Dense and hot neutron star matter is not completely transparent to neutrinos. By taking into account the finite diffusion time, the neutrino trapping scheme limits the loss of energy and lepton number.

In Table 1 maximum and average values of the luminosities ($L_{\nu_i}^{\text{max}}$ and $L_{\nu_i}^{\text{av}}$, respectively, the latter in brackets) in the simulated time intervals are listed for ν_e and $\bar{\nu}_e$ and for the sum of all heavy-lepton neutrinos. The latter are denoted by $\nu_x \equiv \nu_{\mu}, \bar{\nu}_{\mu}, \nu_{\tau}, \bar{\nu}_{\tau}$ and are mainly produced by e^+e^- annihilation. The total neutrino luminosities $L_{\nu}(t)$ (Fig. 3) fluctuate strongly with the varying mass transfer rate to the black hole during the cycles of orbital decay and widening (compare with Fig. 1). The total energy E_{ν} radiated in neutrinos in 10–20 ms is typically several 10^{51} erg. Time averages of the mean energies $\langle \epsilon \rangle$ of the emitted neutrinos are ~ 15 MeV for ν_e , 20 MeV for $\bar{\nu}_e$, and 30 MeV for ν_x . Luminosities as well as mean energies, in particular for smaller black holes, are significantly higher than in case of NS/NS mergers.

At the end of the simulations, several of the BH/NS models have reached a steady state, characterized by only a slow growth of the black hole mass with a nearly constant accretion rate. Corresponding rates \dot{M}_d are given in Table 2 and are several M_{\odot}/s . From these we estimate torus life times $t_{\text{acc}} = M_d/\dot{M}_d$ of 50–150 ms. Values with $>$ and $<$ signs indicate cases where the evolution and emission are still strongly time-dependent at the end of the simulation. In these cases the accretion torus around the black hole has also not yet developed axial symmetry. In all other cases the effective disk viscosity parameter $\alpha_{\text{eff}} \sim v_r/v_{\text{Kepler}} \sim 3\sqrt{6}R_s/(t_{\text{acc}}c)$, evaluated at a representative disk radius of $3R_s = 6GM_{\text{BH}}/c^2$, has the same value, 4 – 5×10^{-3} . This value is associated with the numerical viscosity of the hydro code (which solves the Euler equations) and the chosen resolution. The further disk evolution is driven by the angular momentum transport mediated by viscous shear forces, which determine the accretion rate.

The physical value of the disk viscosity is unknown. The numerical viscosity of our code, however, is in the range where the viscous energy dissipation and the energy emission by neutrinos should be roughly equal, i.e., where the conversion efficiency $q_{\nu} = \langle L_{\nu} \rangle / (\dot{M}_d c^2)$ of rest-mass energy to neutrinos is nearly maximal (see Ruffert et al. 1997; Ruffert & Janka 1999). Assuming that the average neutrino luminosity $\langle L_{\nu} \rangle$ at t_{sim} is

representative for the subsequent accretion phase, we obtain for q_ν numbers between 4 and 6% and total energies $E_\nu \sim \langle L_\nu \rangle t_{\text{acc}}$ around 3×10^{52} erg (Table 2). Annihilation of neutrino pairs, $\nu\bar{\nu} \rightarrow e^+e^-$, deposits energy at rates up to $\dot{E}_{\nu\bar{\nu}} \sim 2 \times 10^{52}$ erg/s in the vicinity of the black hole (Fig. 4). This corresponds to total energies $E_{\nu\bar{\nu}} \sim \dot{E}_{\nu\bar{\nu}} t_{\text{acc}}$ as high as $\sim 10^{51}$ erg and annihilation efficiencies $q_{\nu\bar{\nu}} = \dot{E}_{\nu\bar{\nu}} / \langle L_\nu \rangle$ of 1–3%.

5. CONCLUSIONS

Our simulations confirm BH/NS mergers as possible sources of cosmic GRBs. A large fraction of the neutron star matter is swallowed by the black hole within milliseconds, but a thick disk with a mass of $\sim 0.5 M_\odot$ forms and could be accreted on time scales of about 0.1 s. The region above the poles of the black hole contains definitely less than $10^{-5} M_\odot$ of baryonic matter and an energy deposition of $\sim 10^{51}$ erg by $\nu\bar{\nu}$ annihilation should allow for relativistic expansion with a Lorentz factor $\Gamma = 1 + E_{\nu\bar{\nu}} / (Mc^2) \sim 100$. These estimates should not change much if the different effects of general relativity on $\nu\bar{\nu}$ annihilation are taken into account in combination (Ruffert & Janka 1999). The energy in the pair-plasma could therefore be sufficient to explain observable burst luminosities $L_\gamma \sim E_{\nu\bar{\nu}} / (f_\Omega t_\gamma)$ up to several 10^{53} erg s⁻¹ for burst durations

$t_\gamma \approx 0.1$ –1 s, if the γ emission is beamed in two moderately focussed jets into a fraction $f_\Omega = 2\delta\Omega/(4\pi) \approx 1/100$ –1/10 of the sky. Such a modest amount of beaming (jet opening half-angles between about ten and several ten degrees) has to be expected because the dense gas in the equatorial plane of the accreting black hole prevents relativistic expansion outside a low-density funnel along the system axis. Most likely not all the kinetic energy of the jets is converted to γ photons. More energy, however, could be pumped into the pair-plasma fireball when the black hole rotates rapidly (Popham, Woosley, & Fryer 1999) or magnetic fields help tapping the rotational energy of the accretion torus and of the black hole with higher efficiency than $\nu\bar{\nu}$ annihilation does (Mészáros, Rees, & Wijers 1999; Brown et al. 1999; Lee, Wijers, & Brown 1999). General relativistic simulations of the merging and post-merging phases are very important. A possible runaway instability of the black hole – torus system could be a serious problem of this scenario (Nishida & Eriguchi 1996).

HTJ has been supported by DFG grant SFB 375 für Astro-Teilchenphysik, MR by a PPARC Advanced Fellowship, and CLF by NASA (NAG5-8128) and the US DOE ASCI Program (W-7405-ENG-48).

REFERENCES

Bethe, H.A., & Brown, G.E. 1998, ApJ, 506, 780
 ———. 1999, ApJ, 517, 318
 Blanchet, L., Damour, T., & Schäfer, G. 1990, MNRAS, 242, 289
 Blinnikov, S.I., Novikov, I.D., Perevodchikova, T.V., & Polnarev, A.G. 1984, Sov. Astron. Lett., 10, 177
 Brown, G.E., Wijers, R.A.M.J., Lee, C.-H., Lee, H.K., & Bethe, H.A. 1999, ApJ, submitted (astro-ph/9905337)
 Eberl, T. 1998, Diploma Thesis, Technical University Munich (unpublished)
 Eichler, D., Livio, M., Piran, T., & Schramm, D.N. 1989, Nature, 340, 126
 Fryer, C., Woosley, S.E., & Hartmann D.H. 1999, ApJ, submitted (astro-ph/9904122)
 Fryer, C., Woosley, S.E., Herant, M., & Davies, M.B. 1999, ApJ, 520, 650
 Kluźniak, W., & Lee, W.H. 1998, ApJ, 494, L53
 Lattimer, J.M., & Swesty, F.D. 1991, Nucl. Phys., A535, 331
 Lai, D., Rasio, F.A., & Shapiro, S.L. 1994, ApJ, 423, 344
 Lee, W.H., Kluźniak, W. 1998, ApJ, submitted (astro-ph/9808185)
 Lee, W.H., Kluźniak, W. 1999, MNRAS, submitted (astro-ph/9904328)
 Lee, H.K., Wijers, R.A.M.J., & Brown, G.E. 1999, Phys. Rep., submitted (astro-ph/9906213)
 Mao, S., Narayan, R., & Piran T. 1994, ApJ, 420, 171
 Mészáros, P. 1999, astro-ph/9904038; in: Proc. 19th Texas Symp. on Relativ. Astrophysics & Cosmology, Paris, Dec. 1998
 Mészáros, P., Rees, M.J., & Wijers, R.A.M.J. 1999, New Astronomy, 4, 303
 Narayan, R., Piran, T., & Shemi, A. 1991, ApJ, 379, L17
 Nishida, S., & Eriguchi, Y. 1996, ApJ, 461, 320
 Paczyński, B. 1991, Acta Astronomica, 41, 257
 Podsiadlowski, Ph., Joss, P.C., & Hsu, J.J.L. 1992, ApJ, 391, 246
 Popham, R., Woosley, S.E., & Fryer, C. 1999, ApJ, 518, 356
 Portegies Zwart, S.F. 1998, ApJ, 503, L53
 Rasio, F.A., & Shapiro, S.L. 1994, ApJ 432, 242
 Ruffert, M., Janka, H.-Th., & Schäfer, G. 1996, A&A, 311, 532
 Ruffert, M., Janka, H.-Th., Takahashi, K., & Schäfer, G. 1997, A&A, 319, 122
 Ruffert, M., & Janka, H.-Th. 1999, A&A, 344, 573
 Uryū, K., & Eriguchi, Y. 1999, MNRAS, 303, 329

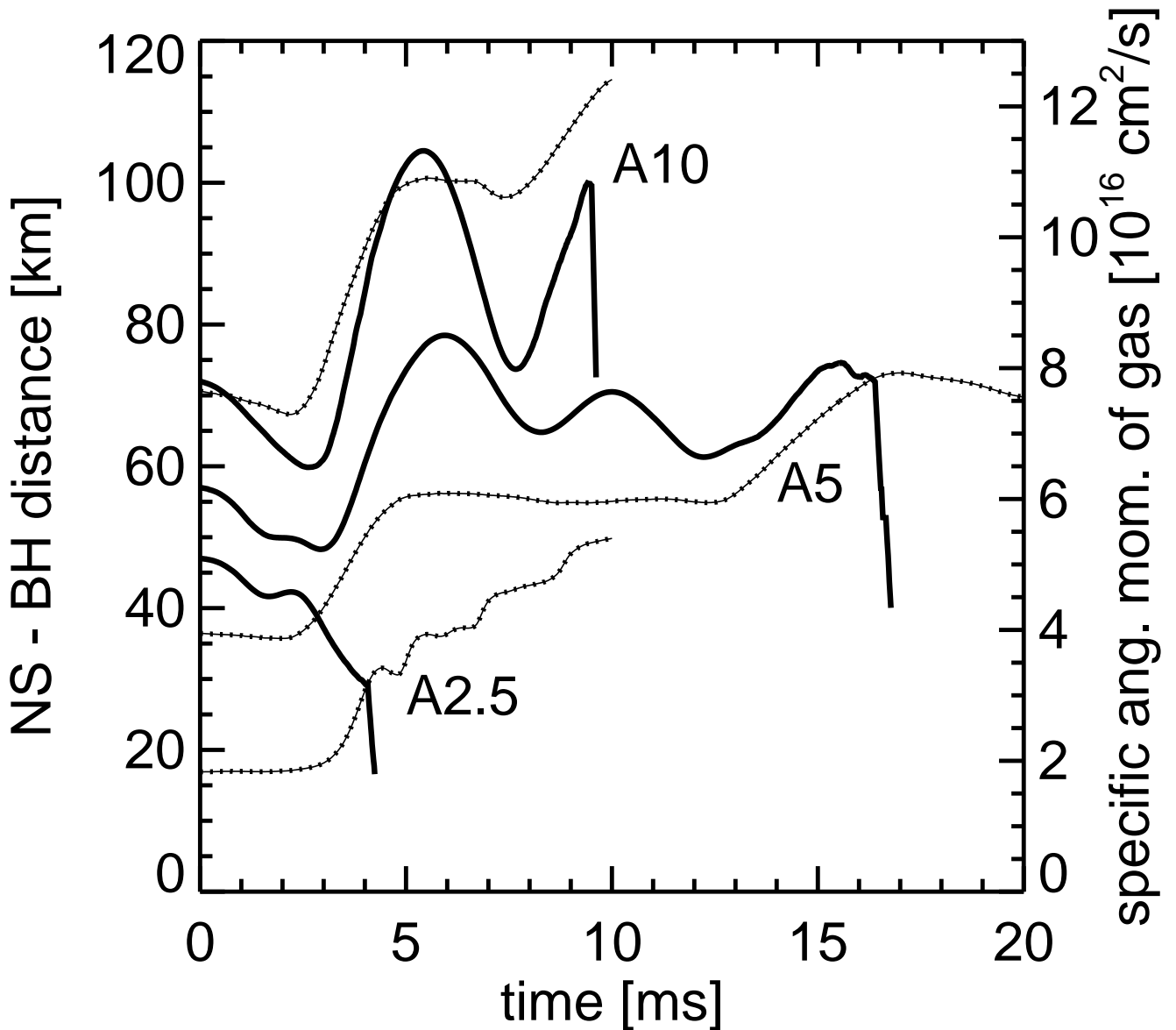


FIG. 1.— Orbital separation between black hole and neutron star (solid lines) and specific angular momentum of the gas on the grid (dotted lines) as functions of time for Models A2.5, A5, and A10. The steep drop at the end of the solid lines marks the moment when the neutron star is disrupted.

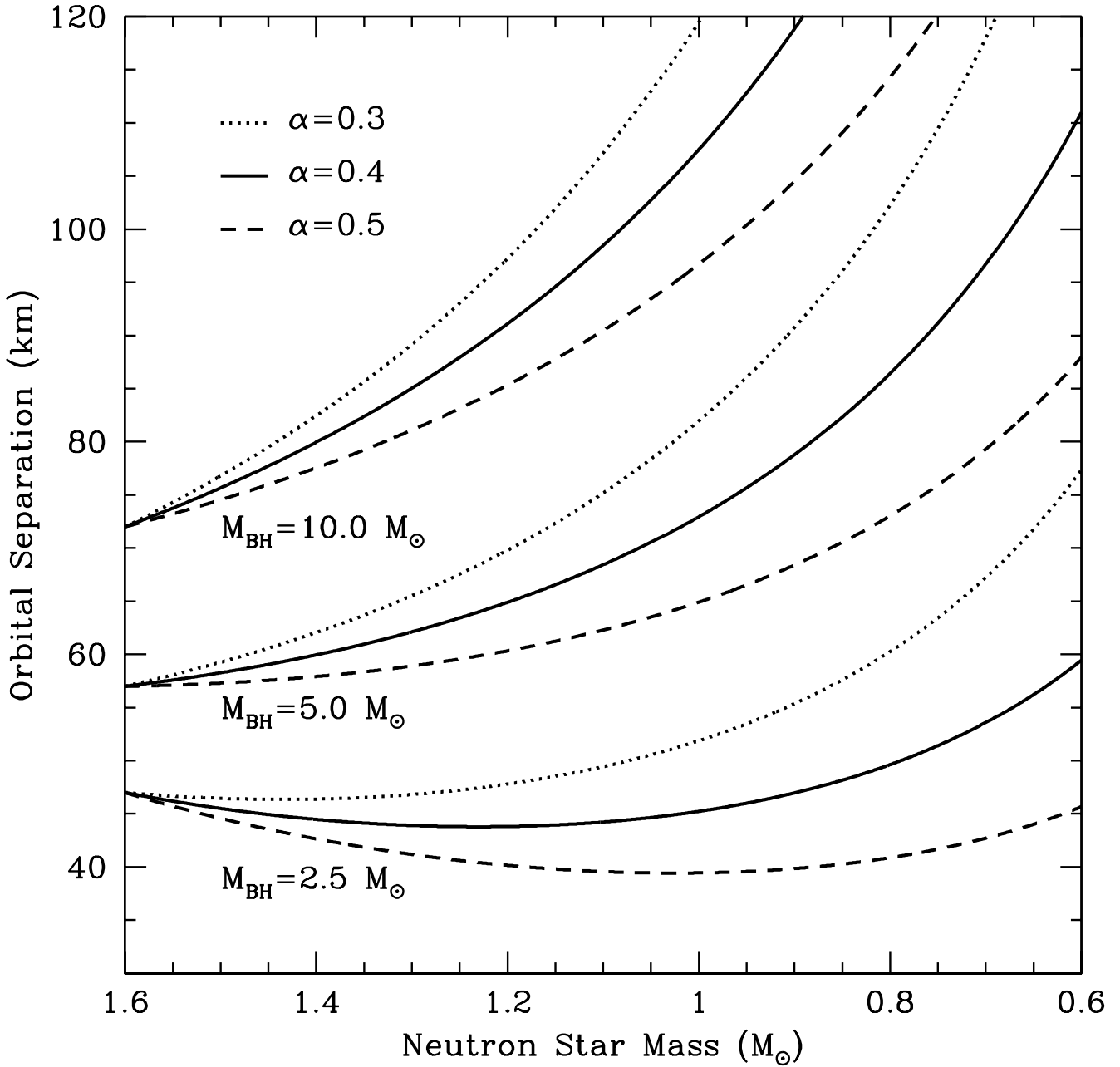


FIG. 2.— Orbital separation as function of neutron star mass for different initial black hole masses and values of parameter α (see text). Note that the effects of GW emission are not included and the total mass of the system, $M_{\text{BH}} + M_{\text{NS}}$ is constant along the lines.

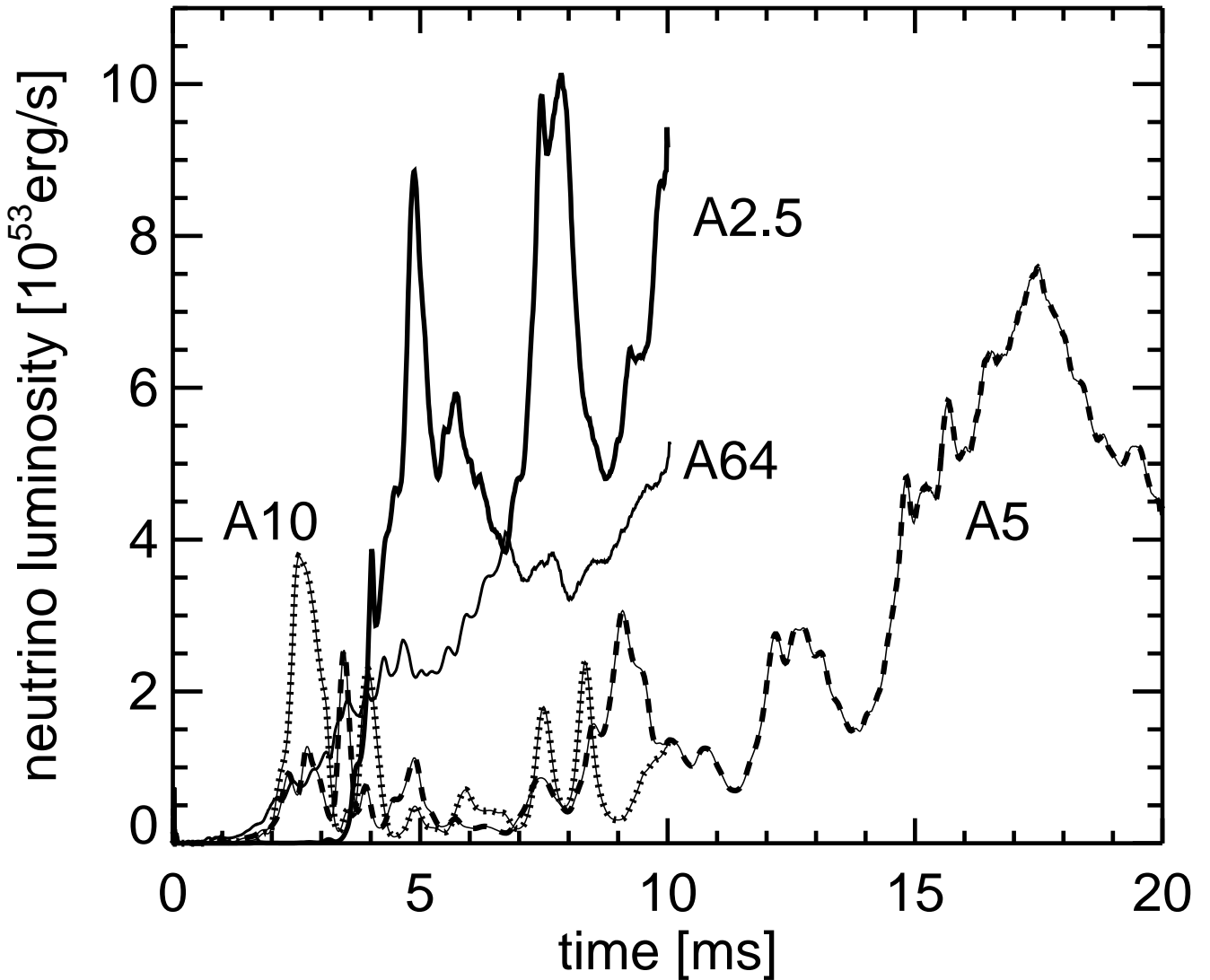


FIG. 3.— Total neutrino luminosities as functions of time for BH/NS merger Models A2.5, A5, and A10, and for the NS/NS merger Model A64.

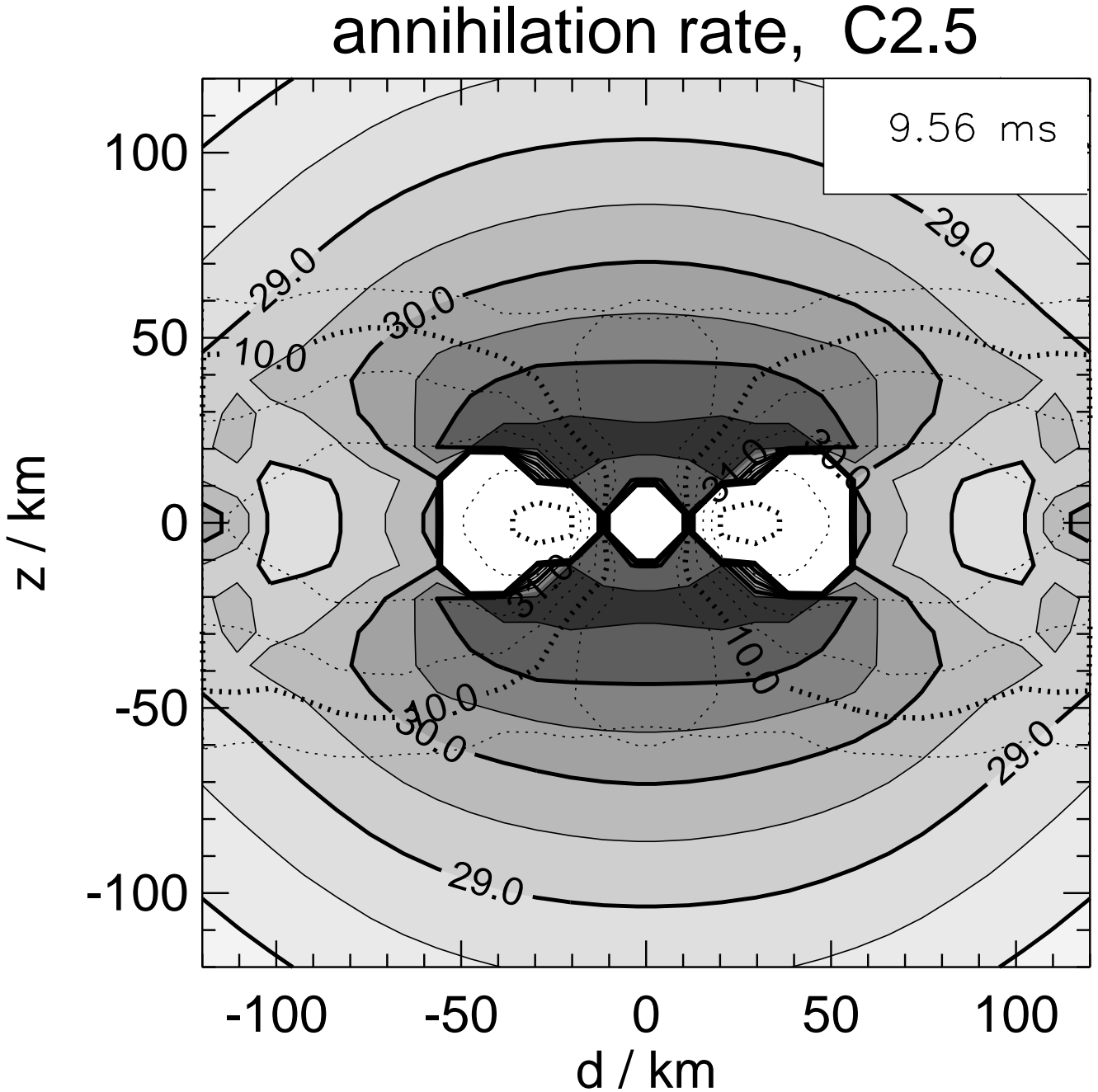


FIG. 4.— Contours of the logarithm of the azimuthally averaged density distribution (dotted lines) of the accretion torus around the black hole (indicated by the white octagonal area at the center) and of the logarithm of the energy deposition rate per cm^3 by $\nu\bar{\nu}$ annihilation into e^+e^- pairs (solid lines) for the BH/NS merger Model C2.5 at time 9.56 ms. The contours are spaced in steps of 0.5 dex. The integral energy deposition rate is $2 \times 10^{52} \text{ erg/s}$.

TABLE 1
GRAVITY WAVES AND NEUTRINOS FROM NS/NS AND BH/NS MERGING

Model	Type	Masses	Spin	t_{sim}	$L_{\text{GW}}^{\text{max}}$	$r h^{\text{max}}$	E_{GW}	$L_{\nu_e}^{\text{max(av)}}$	$L_{\bar{\nu}_e}^{\text{max(av)}}$	$L_{\Sigma\nu_x}^{\text{max(av)}}$	E_{ν}	kT^{max}	$\langle \epsilon_{\nu_e} \rangle$	$\langle \epsilon_{\bar{\nu}_e} \rangle$	$\langle \epsilon_{\nu_x} \rangle$
		(M_{\odot})		(ms)	($10^4 \frac{\text{foe}}{\text{s}}$) ^a	(10^4cm)	(foe)	($100 \frac{\text{foe}}{\text{s}}$)	($100 \frac{\text{foe}}{\text{s}}$)	($100 \frac{\text{foe}}{\text{s}}$)	(foe)	(MeV)	(MeV)	(MeV)	(MeV)
S64	NS/NS	1.2+1.2	solid	10	0.7	5.5	14	0.3(0.2)	0.9(0.5)	0.3(0.2)	0.8	35	12	18	26
D64	NS/NS	1.2+1.8	solid	13	0.4	5.5	13	0.5(0.3)	1.3(0.8)	0.7(0.4)	1.1	35	13	19	27
V64	NS/NS	1.6+1.6	anti	10	1.2	6.0	23	1.1(0.5)	2.6(1.3)	0.7(0.3)	1.9	69	13	19	27
A64	NS/NS	1.6+1.6	none	10	2.1	8.6	52	0.9(0.5)	2.6(1.3)	1.4(0.6)	2.3	39	12	18	26
B64	NS/NS	1.6+1.6	solid	10	2.1	8.9	37	0.6(0.4)	1.8(1.1)	0.9(0.4)	1.8	39	13	19	27
TN10	BH/AD	2.9+0.26	solid	15	0.5(0.4)	1.3(0.9)	0.6(0.2)	0.8	15	9	13	21
C2.5	BH/NS	2.5+1.6	anti	10	2.3	9.9	32	1.5(0.5)	7.3(2.5)	5.2(1.9)	4.5	74	16	22	31
A2.5	BH/NS	2.5+1.6	none	10	2.0	9.9	50	1.8(0.5)	6.4(2.2)	3.1(1.3)	3.6	65	15	22	31
B2.5	BH/NS	2.5+1.6	solid	10	2.1	9.6	61	0.9(0.3)	6.5(1.7)	3.6(0.9)	2.5	61	14	21	29
C5	BH/NS	5.0+1.6	anti	15	3.9	13.0	50	0.7(0.4)	3.8(1.6)	2.5(1.1)	4.5	46	15	20	29
A5	BH/NS	5.0+1.6	none	20	3.2	14.8	102	0.7(0.2)	4.4(1.5)	2.8(0.8)	4.5	51	16	24	31
B5	BH/NS	5.0+1.6	solid	15	3.4	14.5	95	0.6(0.2)	3.7(1.1)	2.5(0.6)	2.9	44	14	21	28
C10	BH/NS	10.0+1.6	anti	10	7.1	21.9	123	0.4(0.1)	2.5(0.4)	1.2(0.1)	0.6	51	14	19	24
A10	BH/NS	10.0+1.6	none	10	6.9	26.2	168	0.2(0.1)	2.5(0.5)	1.2(0.2)	0.7	50	14	20	26
B10	BH/NS	10.0+1.6	solid	10	7.3	26.2	163	0.4(0.1)	2.5(0.8)	1.4(0.2)	1.1	52	13	18	24

^a 1 foe = 10^{51} erg (fifty one erg).

TABLE 2
DISK FORMATION AND NEUTRINO ANNIHILATION

Model	t_{ns}	d_{ns}	$M_{\text{ns}}^{\text{min}}$	ΔM_{ej}	M_{d}	\dot{M}_{d}	t_{acc}	α_{eff}	a_{i}	a_{f}	a_{BH}^{∞}	$\langle L_{\nu} \rangle$	$\dot{E}_{\nu\bar{\nu}}$	q_{ν}	$q_{\nu\bar{\nu}}$	E_{ν}	$E_{\nu\bar{\nu}}$
	(ms)	(km)	(M_{\odot})	($M_{\odot}/100$)	(M_{\odot})	(M_{\odot}/s)	(ms)	(10^{-3})				($100 \frac{\text{foe}}{\text{s}}$) ^a	(foe/s)	(%)	(%)	(foe)	(foe)
S64	2.8	15	...	2.0	0.98	0.75	...	1.5	1	...	1
D64	7.3	15	...	3.8	0.87	0.69	...	2	2	...	1
V64	3.7	15	...	0.0085	0.64	0.49	...	4	9	...	2
A64	1.7	15	...	0.23	0.76	0.55	...	5	9	...	2
B64	1.6	15	...	2.4	0.88	0.63	...	3	7	...	2
TN10	0.26	5	53	4	...	0.42	0.59	1.2	0.5	1.3	0.4	7	0.03
C2.5	2.6	11	0.78	0.01	0.26	6	43	4	0.65	0.47	0.60	7	20	6	3	30	0.9
A2.5	4.3	18	0.78	0.03	0.33	< 14	> 24	< 8	0.67	0.39	0.56	7	20	> 3	3	> 17	> 0.5
B2.5	6.0	23	0.78	0.2	0.45	< 35	> 13	< 14	0.69	0.38	0.61	7	20	> 1	3	> 9	> 0.3
C5	9.1	76	0.40	2.5	0.38	5	76	5	0.44	0.27	0.42	4	8	4	2	30	0.6
A5	16.3	65	0.52	2.5	0.49	6	82	4	0.45	0.17	0.37	4	8	4	2	33	0.7
B5	10.8	79	0.50	5.6	0.45	6	75	5	0.46	0.19	0.38	4	8	4	2	30	0.6
C10	8.0	96	0.65	2.2	0.67	< 10	> 67	< 11	0.24	0.07	0.25	2	2	> 1	1	> 13	> 0.1
A10	9.3	95	0.60	3.2	0.56	< 60	> 9	< 82	0.25	0.07	0.22	2	2	> 0.2	1	> 2	> 0.02
B10	5.1	97	0.65	10.0	0.47	3	160	5	0.25	0.11	0.23	2	2	4	1	32	0.3

^a 1 foe = 10^{51} erg (fifty one erg).